Available online at www.sciencedirect.com
SCIENCE DIRECT®
International Journal of Heat and Mass Transfer 47 (2004) 2073–2083
International Journal of HEAT and MASS TRANSFER
www.elsevier.com/locate/ijhmt

Boundary conditions and wall effect for forced convection heat transfer in sintered porous plate channels

Pei-Xue Jiang *, Meng Li, Yong-Chang Ma, Ze-Pei Ren

Department of Thermal Engineering, Tsinghua University, Beijing 100084, People's Republic of China

Received 5 June 2003; received in revised form 11 December 2003

Abstract

Forced convection heat transfer of water and air in plate channels filled with sintered bronze porous media was simulated numerically using a local thermal non-equilibrium model with consideration of the wall effect caused by heat conduction in the plate wall and in the unheated section of the sintered porous media. The numerical model was used to analyze the effects of the assumed boundary conditions, the porosity at the wall and the wall effect caused by the heat conduction. The results showed that the wall porosity in sintered porous media is less than that in non-sintered packed beds, which intensifies the convection heat transfer in sintered porous media. The wall effect reduces the heat transfer coefficient near the front of the heated section and slightly increases the heat transfer coefficient near the end of the heated section. Numerical simulations of convection heat transfer of air and water in sintered bronze porous media using the local thermal non-equilibrium model and the variable porosity model with consideration of the wall effect corresponded well to the experimental data.

Keywords: Forced convection heat transfer; Porous media; Boundary conditions; Wall effect; Local thermal non-equilibrium; Porosity

1. Introduction

Fluid flow and convection heat transfer in porous media have been widely investigated experimentally and numerically for many years due to the many important applications such as geothermal energy extraction, catalytic and chemical particle beds, petroleum processing, transpiration cooling, solid matrix or micro-porous heat exchangers, packed-bed regenerators, heat transfer enhancement, micro-thrusters, and many others. There have been numerous investigations with theoretical analyze and numerical simulations of convection heat transfer in fluid-saturated porous media. Vafai and Tien [1] investigated the nature and importance of the boundary and inertial effects on the flow and heat transfer in porous media. They showed that for the flow field, the boundary effects are confined to a very thin momentum boundary layer and often have no significant effect on the overall flow field. The effect of the boundary on the heat transfer, however, can be quite important. The inertial effects increase with higher permeability and lower fluid viscosity. The velocity gradients near the wall are then bound to increase, thereby increasing the viscous resistance due to the boundary. Lage [2] described the development of the fundamental processes for flow through porous media from the Darcy equation to turbulence, and presented detailed insight into the effect of turbulence in porous media. The Darcy–Brinkman–Forchheimer model has been widely used in numerical simulations of forced or mixed convection heat transfer in saturated porous media. Results have shown that the transverse thermal dispersion plays a very important role in the convection heat transfer in porous media, while the axial thermal dispersion has little effect [3,4]. The additional thermal conductivity resulting from the thermal dispersion can be expressed as an linear function of Reynolds number in fluid flows with high Reynolds numbers [3], but the constant in the thermal dispersion model is not unique in different

* Corresponding author. Tel.: +86-10-62772661; fax: +86-10-62770209.
E-mail address: jiangpx@te.tsinghua.edu.cn (P.-X. Jiang).

0017-9310/$ - see front matter © 2004 Elsevier Ltd. All rights reserved.
doi:10.1016/j.ijheatmasstransfer.2003.12.003

Nomenclature

c_{pf}	fluid specific heat, J/(kgK)
d_p	particle diameter, m
F	inertia coefficient
G	mass flow rate, kg/s
h	plate channel height, m
h_f	fluid enthalpy, J/kg
h_x	local heat transfer coefficient, W/(m^2 K)
h_{sf}	heat transfer coefficient between solid particles and fluid in porous media, W/(m^2 K)
h_v	volumetric heat transfer coefficient between solid particles and fluid in porous media W/(m^3 K)
K	porous medium permeability, m^2
l_{in}	inlet section length, m
l_h	heated section length, m
l_{out}	outlet section length, m
Nu_{sf}	Nusselt number for convection heat transfer between the solid particles and the fluid in porous media
p	local pressure, Pa
Pr	Prandtl number
Re	Reynolds number
T_f	fluid temperature, K
T_s	solid phase temperature, K
u_0	inlet fluid velocity, m/s
u_p	pore velocity in the x direction, m/s
v_p	pore velocity in the y direction, m/s
U_p	absolute pore velocity ($U_p = (u_p^2 + v_p^2)^{1/2}$), m/s
x, y	coordinates, m

Greek symbols

λ	thermal conductivity, W/(m K)
ρ_0	inlet fluid density, kg/m^3
ρ_f	fluid density, kg/m^3
μ_e	effective absolute viscosity ($\approx\mu_f$), N s/m^2
μ_f	absolute viscosity, N s/m^2
ε	porosity
ε_m	mean porosity
ε_∞	porosity at channel center

Subscripts

b	bulk mean temperature
d	dispersion
f	fluid
m	mean or effective
p	pore or particle
s	solid
w	wall

references [3,5–7]. A modified model for the additional thermal conductivity resulting from the transverse thermal dispersion was presented by Jiang et al. [8]. A further modification of the transverse thermal dispersion model was then developed [9] with a unified expression for the constant in the thermal dispersion model.

The theoretical and numerical investigations of convection heat transfer in porous media have used two different models for the energy equation: the local thermal equilibrium model and the local thermal non-equilibrium model. Lage [10] examined the issue of boundary conditions and thermal equilibrium on a fully saturated porous medium for steady conduction through a porous layer. When a uniform heat flux condition was imposed at both boundaries of the layer, the phases were in thermal equilibrium only if $\lambda_f = \lambda_s$. If the boundary temperatures of the phases are equal, the entire saturated porous medium will be in thermal equilibrium. Although for most practical situations thermal equilibrium will prevail in most of the layer, the thermal non-equilibrium at the heated boundary can drastically affect the measurement of the effective thermal conductivity of the medium. In recent years the local thermal non-equilibrium model has been used more frequently in the energy equation in theoretical and numerical research on convection heat transfer in the porous media [8,9,11–20] to more accurately model the convection heat transfer processes in porous media. With the thermal non-equilibrium model, the treatment of the boundary conditions for the energy equation significantly affects the numerical simulation results. A number of papers have analyzed this problem, e.g. Amiri et al. [12], Jiang et al. [9,18,19], Quintard [13], Peterson and Chang [14], Martin et al. [15], Lee and Vafai [16], and Alazmi and Vafai [20]. For the constant heat flux boundary condition there are several different methods to treat the energy equation boundary conditions. The main difference among them is whether the fluid temperature is equal to the solid phase temperature at the boundary surface. Jiang et al. [18,19] investigated the various treatments of the constant heat flux boundary conditions by comparing the numerical results with experimental data for water and air in porous media. They concluded that the convection heat transfer of water and air in non-sintered porous media can be best predicted numerically using the thermal non-equilibrium model with the ideal constant wall heat flux boundary condition which assumes that the heat fluxes into the liquid and into the porous matrix are the same. Alazmi and Vafai [20] analyzed eight different forms of constant wall heat flux boundary conditions in the absence of local thermal equilibrium conditions in porous media.

They found that the different boundary conditions may lead to substantially different results. At the same time, they pointed out that no single model is correct in all situations since previous studies validated each of the two primary models. In addition, the mechanics of splitting the heat flux between the two phases is not yet resolved.

Jiang [21] numerically analyzed the heat transfer boundary characteristics on the surface between a thin plate and a solid particle in contact with the plate with convection heat transfer due to water or air and a constant heat flux on the outer plate wall. The analysis studied the influence of the thermal contact resistance between the plate wall and the solid particle and the wall thickness on the surface thermal characteristics. The results showed that when the thermal conductivities of the fluid and the solid particle were similar, the temperature and heat flux distributions on the contact surface between the thin plate and the particle and on the convection heat transfer surface of the thin plate near the particle were quite uniform, which means that local thermal equilibrium exists for such conditions. If the thermal contact resistance on the wall surface between the solid particles and the plate wall is considered, the solid particle temperature on the contact surface and the fluid temperature on the convection heat transfer surface of the thin plate near the particle are significantly different, while the heat fluxes transferred through the solid particles and the fluid adjacent to the surface are similar. If the thermal contact resistance on the wall surface between the solid particles and the wall is not considered and the plate is relatively thick (e.g. 1–2 mm), the heat fluxes through the solid particles and the fluid near the wall are significantly different, while the temperatures of the solid particles and the fluid near the wall are fairly close, that is $T_{fw} \approx T_{sw}$. The analytical results in Jiang [21] were then used to further investigate the forced convection heat transfer in plate channels filled with non-sintered metallic or non-metallic particles (packed beds) or sintered porous media using a non-thermal equilibrium model [9]. The numerical results were compared with experimental data from Jiang et al. [19,22] and Hwang and Chao [23] to analyze the effects of the assumed boundary conditions for the different convection heat transfer processes in non-sintered porous media and in sintered porous media. The results showed that the numerical simulation of the convection heat transfer of air and water in non-sintered packed beds using a local thermal non-equilibrium model with the assumption that the heat fluxes transferred by the solid phase and the fluid on the heat transfer surface were the same with a variable porosity model agreed well with the experimental data. In addition, the convection heat transfer coefficient in sintered porous media is much higher than that in packed beds. Jiang et al. [9] also showed that for numerical simulation of convection heat transfer in sintered porous media, the boundary conditions on the wall should be that the particle temperatures are equal to the fluid temperatures.

The present paper numerically investigates the forced convection heat transfer of water and air in plate channels filled with sintered bronze particles using a non-thermal equilibrium model with an improved energy equation for the solid phase and an improved wall porosity model with consideration of the wall effect caused by the heat conduction in the plate wall and in the unheated section of the sintered porous media. The simulation results are compared with new experimental results [24] to analyze the effects of the assumed boundary conditions, the porosity at the wall and the wall effect caused by the heat conduction.

2. Physical model, governing equations and numerical method

Fig. 1 shows the physical model used in the present numerical simulation, which is similar to the test section

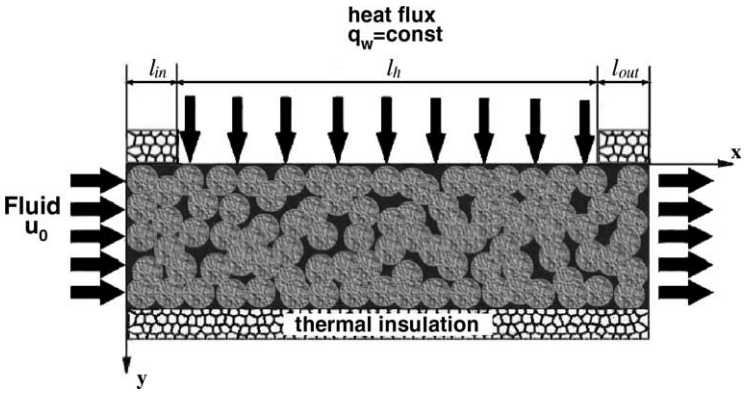

Fig. 1. Physical model and coordinate system.

in the experimental research [24]. The analysis assumes that the porous media is homogeneous and isotropic. The upper plate of the channel receives a constant heat flux, q_w, while the lower plate is adiabatic. Two adiabatic sections are placed before and after the heated section. Fluid flow enters the channel with a uniform velocity, u_0, and constant temperature, T_{f0}. The fluid flow is single-phase and two-dimensional, steady, and non-Darcian flow. The analysis assumes that the test section width, W, is much larger than the height, h (in the experimental research [24] $h = 10$ mm and $W = 120$ mm), so that all conditions are uniform across the width and the problem can be analyzed as a two-dimensional problem. Longitudinal conduction in the fluid and the pressure variation in the y direction are assumed to be negligible, but longitudinal conduction in the solid phase is included.

The steady-state, two-dimensional governing equations for single-phase convection heat transfer in an isotropic, homogeneous porous medium based on the Brinkman–Darcy–Forchheimer model with consideration of variable properties, variable porosity, thermal dispersion, viscous dissipation, and local thermal non-equilibrium, but neglecting the longitudinal thermal conduction in the fluid, can be written in the following form [8,18]:

$$\frac{\partial(\rho_f \varepsilon u_p)}{\partial x} + \frac{\partial(\rho_f \varepsilon v_p)}{\partial y} = 0 \tag{1}$$

$$\frac{\partial(\rho_f \varepsilon u_p u_p)}{\partial x} + \frac{\partial(\rho_f \varepsilon v_p u_p)}{\partial y} = -\frac{\partial(\varepsilon p_p)}{\partial x} - \frac{\varepsilon^2 \mu_f}{K} u_p - \varepsilon^3 \frac{\rho_f F}{\sqrt{K}} |U_p| u_p + \frac{\partial}{\partial y}\left(\varepsilon \mu_e \frac{\partial u_p}{\partial y}\right) \tag{2}$$

$$\int_0^h \rho_f \varepsilon u_p \, dy = \rho_0 u_0 h \tag{3}$$

$$\frac{\partial(\rho_f \varepsilon u_p h_f)}{\partial x} + \frac{\partial(\rho_f \varepsilon v_p h_f)}{\partial y} = \frac{\partial}{\partial y}\left[\frac{(\varepsilon\lambda_f + \lambda_d)}{C_{pf}} \cdot \frac{\partial h_f}{\partial y}\right] + \frac{\varepsilon^2 \mu_f}{K} u_p^2 + \frac{\varepsilon^3 \rho_f F}{\sqrt{K}} |U_p| u_p^2 + h_v (T_s - T_f) \tag{4}$$

$$\frac{\partial}{\partial x}\left[\lambda_s (1-\varepsilon)\frac{\partial T_s}{\partial x}\right] + \frac{\partial}{\partial y}\left[\lambda_s (1-\varepsilon)\frac{\partial T_s}{\partial y}\right] - h_v (T_s - T_f) = 0 \tag{5}$$

The parameters used in Eqs. (1)–(5) were taken from Hunt and Tien [25], Hsu and Cheng [3], Amiri and Vafai [11], Cheng and Hsu [26], Achenbach [27] and Kar and Dybbs [28]:

$$K = d_p^2 \varepsilon^3 / (150(1-\varepsilon)^2);$$

$$F = 1.75/(\sqrt{150}\varepsilon^{3/2});$$

$$\frac{\lambda_m}{\lambda_f} = \left[1 - \sqrt{1-\varepsilon}\right] + \frac{2\sqrt{1-\varepsilon}}{1-\sigma B}\left[\frac{(1-\sigma)B}{(1-\sigma B)^2} \ln\left(\frac{1}{\sigma B}\right) - \frac{B+1}{2} - \frac{B-1}{1-\sigma B}\right];$$

$$B = 1.25((1-\varepsilon)/\varepsilon)^{10/9}; \quad \sigma = \lambda_f/\lambda_s \tag{6}$$

$$Nu_{sf} = h_{sf} d_p/\lambda_f = [(1.18Re^{0.58})^4 + (0.23Re_h^{0.75})^4]^{1/4}$$
$$h_v = h_{sf} \cdot 6(1-\varepsilon)/d_p; \quad Re = \varepsilon \rho u_p d_p/\mu \tag{7}$$
$$Re_h = Re/(1-\varepsilon)$$

$$h_{sf} = 0.0040(\lambda_f/d_v) Pr_f^{0.333} Re^{1.35} \quad Re_d < 100$$
$$h_{sf} = 0.0156(\lambda_f/d_v) Pr_f^{0.333} Re^{1.04} \quad Re_d \geqslant 100 \tag{8}$$
$$h_v = a h_{sf}; \quad a = 20.346 \times (1-\varepsilon)\varepsilon^2/d_p$$
$$Re = \varepsilon \rho u_p d_v/\mu; \quad d_v = 4\varepsilon/a$$

Thermal dispersion is a very important characteristic of flow in porous media and is one of the main reasons for the enhanced heat transfer. The additional thermal conductivity resulting from the thermal dispersion in porous media can be expressed as [3]:

$$\lambda_d = C(\rho c_p)_f \cdot d_p \sqrt{u_p^2 + v_p^2}(1-\varepsilon) \tag{9}$$

The constant C in Eq. (9) is an important parameter which strongly affects the numerical simulation accuracy. For non-sintered porous media a modified model for the constant C was developed by comparing the numerical simulation results with experimental data for water in a glass particle packed bed [8]. The analysis assumes that the modifications developed by Jiang et al. [9] for the model for C can also be used for sintered porous media:

$$C = 1.60[Re_p \cdot Pr_f \cdot (1-\varepsilon_m)]^{-0.8282} \tag{10}$$

The present model uses Eqs. (9) and (10) to calculate the additional thermal conductivity resulting from the thermal dispersion in sintered porous media.

The boundary conditions and the calculation method for the porosity in the sintered porous structure will be described in Section 3.

Energy will be transported along the axial direction in the solid phase and in the plate wall. Analysis of the wall temperature and the energy balance in the experimental and numerical studies showed that energy loss occurs along the wall near the test section inlet and outlet, which is referred to as the wall effect, Fig. 2. Numerical simulations without consideration of the wall effect differ significantly from the experimental data near the inlet and outlet. Therefore, unheated sections ($l_{in} = l_{out} = 5$ mm) were added to the test section inlet

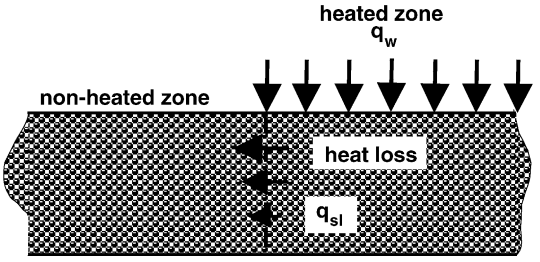

Fig. 2. Heat conduction wall effect.

and outlet in the numerical simulation to model the wall effect.

The numerical method was similar to that used by Jiang et al. [8] except that the thermophysical properties were assumed to vary with pressure as well as with temperature and the calculational region including the unheated inlet and outlet section as well as the heated section. The property values were calculated from tabular values using second-order interpolation relative to both the temperature and pressure. The variation of the fluid thermophysical properties with pressure was based on the calculated pressure drop along the channel relative to the known outlet pressure (usually close to 1 atm). The algorithm assumed an inlet pressure and then calculated the pressure drop for the entire channel length. The inlet pressure was then set equal to the outlet pressure plus the pressure drop in the test section. The procedure was then repeated until all of the convergence criteria were satisfied. The convergence criteria used in the present study were: the relative errors of the longitudinal velocity u_p, the fluid enthalpy h_f and the solid phase temperature T_s were less than 10^{-4}; the relative errors of the longitudinal pressure gradients $\partial p/\partial x$ were less than 5×10^{-3}; the relative errors of the velocity v_p were less than 10^{-2} due to its small values compared with the longitudinal velocity u_p. In the numerical analysis, the convection heat transfer in the inlet section, the heated section and the outlet section were calculated assuming that the heat fluxes on the inlet and the outlet section surfaces were zero or varied as a function of x as shown in Section 3.3. Analysis of the grid independence showed that for an adequate distribution of grid points, the numerical results did not depend on the number of grid points (e.g., 240×52, 240×102, 240×202, 140×102 and 340×102). Therefore, a non-uniform grid was employed with 102 grid points normal to the wall and 200 grid points along the heated section, 20 grid points along the inlet section and 20 grid points along the outlet section in the axial direction.

The local heat transfer coefficient on the upper wall surface was evaluated as

$$h_x = \frac{q_w}{T_w(x) - T_{fb}(x)} \tag{11}$$

3. Boundary conditions, porosity model and numerical simulation of the wall effect

For single-phase convection heat transfer in an isotropic and homogeneous non-sintered porous medium (packed bed), the numerical results using the steady-state, two-dimensional governing equations based on the Brinkman–Darcy–Forchheimer model with consideration of variable properties, variable porosity, thermal dispersion, viscous dissipation, and local thermal non-equilibrium corresponded well to experimental data [8,9,18,19]. The effective thermal conductivity of the sintered porous media was larger than that in non-sintered porous media using the same materials [24] and the porosity distributions in the sintered and non-sintered porous media were also different. Therefore, the variable porosity model and the boundary conditions were modified for the numerical simulation of convection heat transfer in sintered porous media.

3.1. Boundary conditions

As shown by Jiang [21], the thermal contact resistance on the wall surface between the solid particles and the plate wall in non-sintered porous media would result in the solid particle temperature on the contact surface being significantly different from the fluid temperature at the convection heat transfer surface of the thin plate near the particle, while the heat fluxes transferred through the solid particles and the fluid adjacent to the surface were similar. The boundary conditions for the numerical simulations of convection heat transfer in non-sintered porous medium (packed bed) were discussed earlier [8,9,18,19].

Jiang [21] showed that if the thermal contact resistance on the wall surface between the solid particles and the wall is negligible as would occur in sintered porous media and the wall is relatively thick (e.g. 1–2 mm), the heat fluxes through the solid particles and the fluid near the wall are significantly different, while the temperatures of the solid particles and the fluid near the wall are fairly close, that is $T_{fw} \approx T_{sw}$. Therefore, the following boundary conditions were used for the analysis of the heat transfer in sintered porous media:

$$\begin{aligned}
&x = 0 \text{ and } 0 < y < h: \quad u = u_0, \quad v = 0,\\
&T_f = T_{f0}, \quad \frac{\partial T_s}{\partial x} = 0\\
&x = l_{in} + l_h + l_{out} \text{ and } 0 < y < h: \quad \frac{\partial T_s}{\partial x} = 0\\
&y = 0 \text{ and } 0 < x < l_{in} + l_h + l_{out}: \quad u_p = v_p = 0,\\
&T_f = T_s, \quad q_w = \lambda_m \frac{\partial T_f}{\partial y}\bigg|_w\\
&y = h \text{ and } 0 < x < l_{in} + l_h + l_{out}: \quad u_p = v_p = 0,\\
&T_f = T_s, \quad \frac{\partial T_f}{\partial y} = 0
\end{aligned} \tag{12}$$

3.2. Porosity model

Observation of a cross section of the sintered bronze porous plate channel showed that the sintering process fused the particles to each other and to the plate wall and deformed the particles. The fusion between the particles with the plate wall reduced the porosity near the wall relative to the non-sintered porous media where ε_w is close to 1. The porosity in the sintered porous channel was measured from several two-dimensional slices of the sintered porous plate channel as shown in Fig. 3 to determine the average porosity distribution at each height shown in Fig. 4.

The data in Fig. 4 show that the porosity at the wall in the sintered porous plate channel, ε_w, was about 0.8. The variable porosity model used in the present paper was therefore [8]:

$$\begin{aligned} \varepsilon &= \varepsilon_\infty \lfloor 1 + a e^{-6y/d_p} \rfloor, \quad 0 \leqslant y \leqslant h/2 \\ \varepsilon &= \varepsilon_\infty [1 + a e^{-6(h-y)/d_p}], \quad h/2 \leqslant y \leqslant h \end{aligned} \tag{13}$$

Here, $a = \frac{\varepsilon_w}{\varepsilon_\infty} - 1$ and ε_m is defined as $\varepsilon_m = \frac{h}{2}\int_0^{h/2} \varepsilon \, dy$. In the numerical calculations, ε_∞ was determined iteratively using ε_w and ε_m.

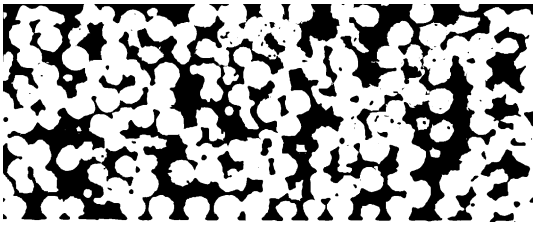

Fig. 3. Two-dimensional slice of the sintered porous plate channel ($d_p = 1.0$–1.4 mm).

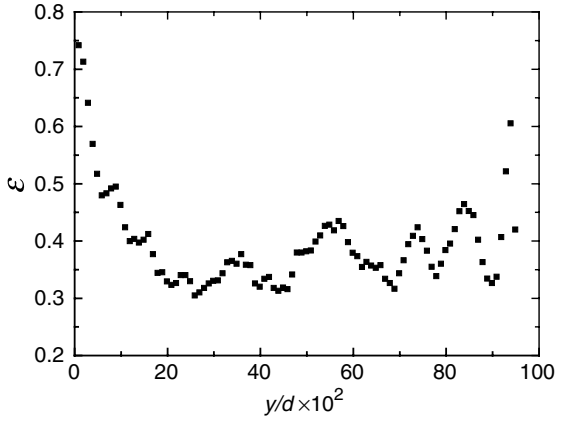

Fig. 4. Average porosity distribution in the sintered porous channel ($d_p = 1.0$–1.4 mm).

The numerical results for $\varepsilon_w = 0.5$, $\varepsilon_w = 0.8$ and $\varepsilon_w = 0.99$ are compared with the experimental data in the sintered porous plate channel in Fig. 5. For the porosity at the wall of 0.8, the numerical results agree well with the experimental data, but for porosities at the wall of 0.5 or 0.99, the numerical results differ greatly from the experimental data. Therefore, the measured porosity at the wall of 0.8 produced the best agreement between the numerical and experimental results.

The porosity at the wall and the thermal contact resistance are important factors affecting the heat transfer from the wall surface into the solid phase in the porous media. If the porosity at the wall is less than the usual porosity near the wall for non-sintered porous media which is close to unity and if there is no thermal contact resistance between the particles and the wall, the heat transport from the wall into the porous media is more intense which enhances the overall heat transfer coefficient on the plate wall. The influence of the porosity at the wall and the thermal contact resistance on the overall convection heat transfer is more evident

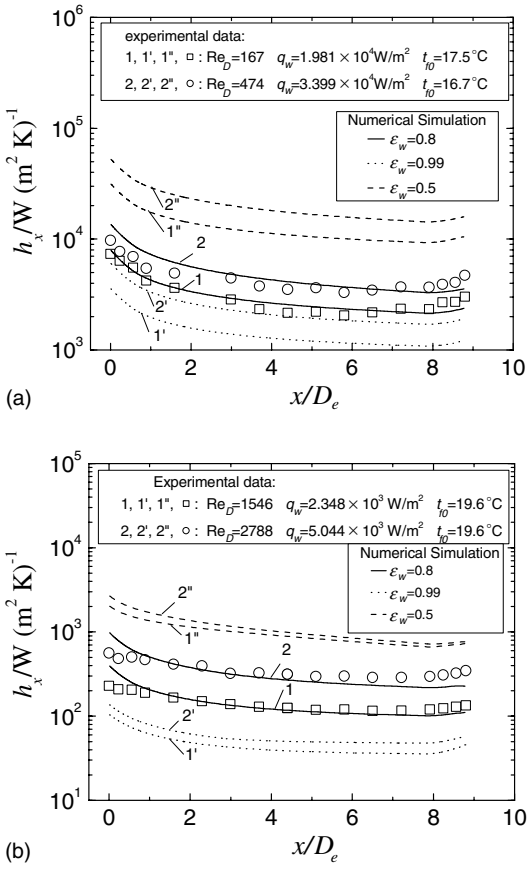

Fig. 5. Comparison of numerical results with experimental data in the sintered porous plate channel for different porosities at the wall for (a) water and (b) air ($d_p = 0.5$–0.71 mm).

for fluids with low thermal conductivities. Therefore, the convection heat transfer with air in sintered porous media is much more intense than in non-sintered porous media, but the difference between the convection heat transfer with water in sintered porous media and in non-sintered porous media is not very large [24].

3.3. Wall effect

In the numerical simulation, a variable heat flux, $q_w = 0.2q_{w0}e^{x/x_{in}}$, was added to the inlet section to model the actual heat flux in the experimental test section with the corresponding heat flux subtracted from the heated section along the same length as in the inlet section. The same procedure was used for the outlet section. The function $q_w = 0.2q_{w0}e^{x/x_{in}}$ approximates the actual heat flux distribution. The local heat transfer coefficient calculation using Eq. (11) still used the constant heat flux assumption to coordinate with the experimental data reduction. The numerical results in Fig. 6 show that the model with the wall effect more closely represents the experimental data.

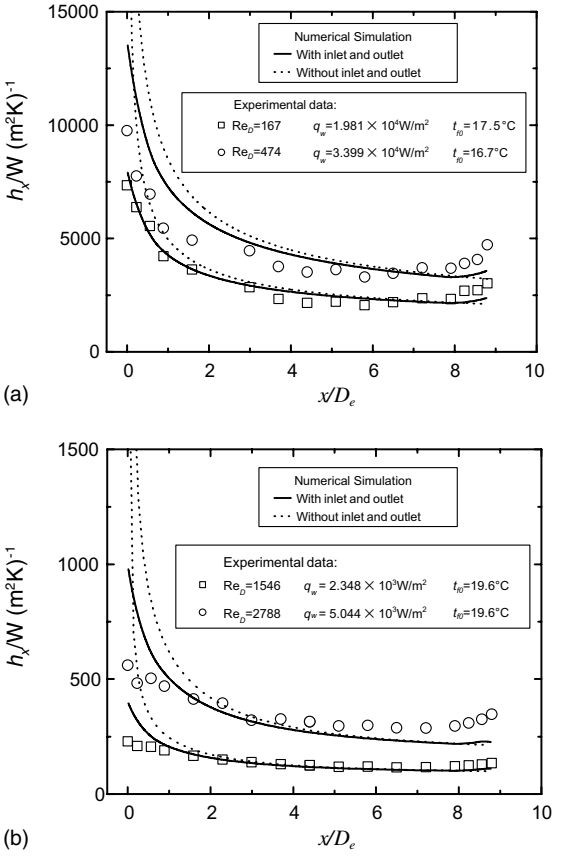

Fig. 6. Edge effect in the sintered porous plate channel for (a) water and (b) air (d_p = 0.5–0.71 mm).

In the experiments the fluid was heated in the inlet section before entering the heated section due to axial heat conduction in the upper plate wall and in the sintered porous media; therefore, a thermal boundary formed along the porous plate channel before entering the heated section. The convection heat transfer coefficient in the developing thermal boundary layer decreased sharply; therefore, the experimental results for the convection heat transfer coefficient near the heated section inlet were less than the predicted results. At the heated section outlet, the wall temperature decreased due to axial heat conduction to the outlet section. The data reduction assumed a constant heat flux to calculate the heat transfer coefficient along all of the heated section; therefore, the experimental heat transfer coefficient gradually increased near the heated section outlet. The numerical simulation in the present paper with consideration of the wall effect followed this tendency. However, this method for analyzing the wall effect is still an approximation. A more accurate method would be to calculate the combined convection heat transfer in the porous plate channel and the thermal conduction in the plate wall. The wall effect must be included since it strongly influences the heat transfer in the experiments and in the numerical calculations.

4. Numerical simulation results and discussion

Convection heat transfer in sintered bronze porous media was simulated numerically for flow in a test section in [24] which was 188 mm long by 120 mm wide by 10 mm high. The boundary conditions given in Eq. (12) and the variable porosity model in Eq. (13) were used in the numerical model which also included the wall effect in the inlet and outlet sections. The particle diameters in the tests were 0.5–0.71, 1.2–1.4 and 1.4–2.0 mm. The thermal conductivity of the bronze particle material was assumed to be 54 W/(m K).

Figs. 7 and 8 present the numerical results for the local heat transfer coefficient for water and air in the sintered bronze porous channel with the corresponding experimental data. The numerical results in the present paper with consideration of the wall effect are quite close to the experimental data. The results in Figs. 7 and 8 show some differences between the convection heat transfer coefficient from the numerical and experimental results especially for large values of x. One reason is that the method for analyzing the wall effect in the present study is still an approximation. A more accurate method will be used in further research. The second reason may be that some of the parametric models used in the present study such as the effective thermal conductivity (Eq. (6)), the convection heat transfer coefficient between the particles and the fluid (Eqs. (7) and (8)), the additional thermal conductivity resulting from the

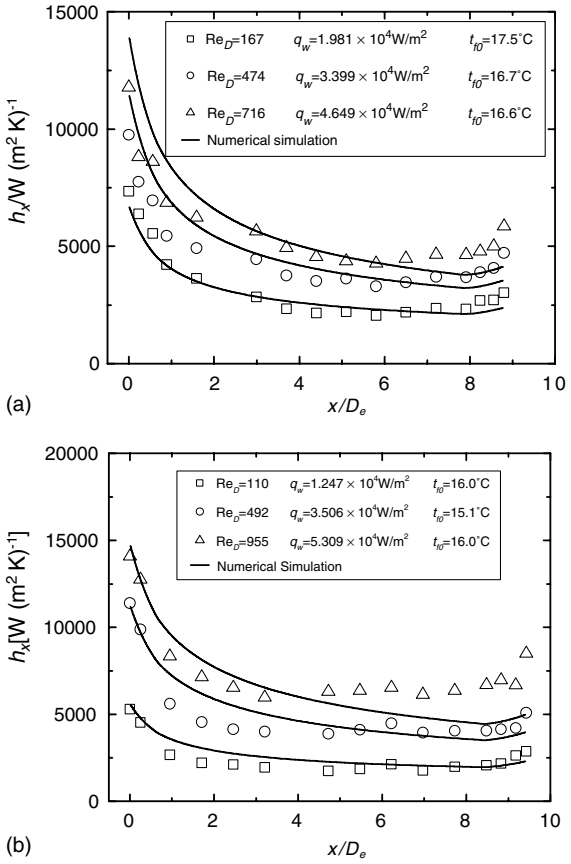

Fig. 7. Numerical results and experimental data for the local heat transfer coefficient for water in the sintered bronze porous channel: (a) $d_p = 0.5$–0.71 mm; (b) $d_p = 1.0$–1.4 mm.

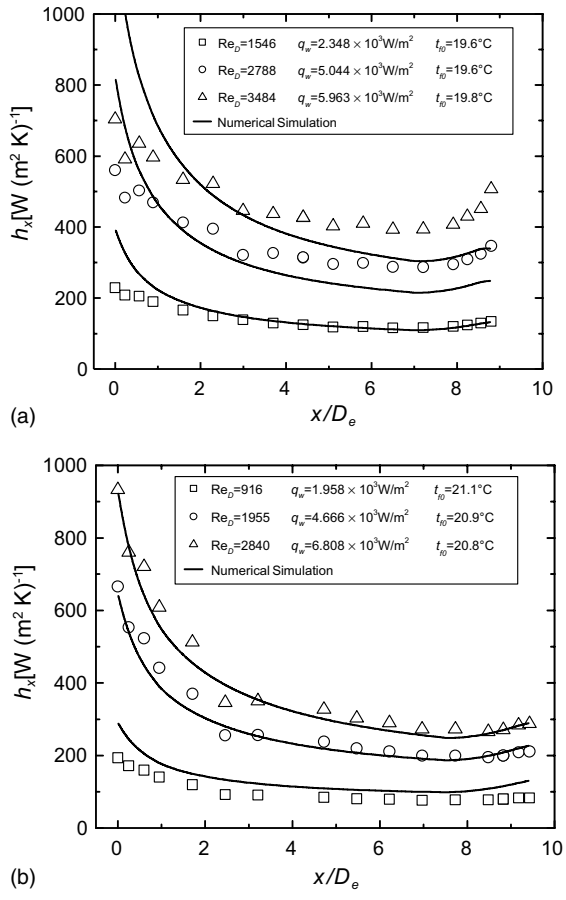

Fig. 8. Numerical results and experimental data for the local heat transfer coefficient for air in the sintered bronze porous channel: (a) $d_p = 0.5$–0.71 mm; (b) $d_p = 1.0$–1.4 mm.

thermal dispersion (Eq. (9) and (10)), the boundary condition model, and even the porous medium permeability, K, and the inertial coefficient, F, need to be improved.

Figs. 9 and 10 present the distributions of the solid phase temperature and the fluid temperature for convection heat transfer of water and air in sintered porous media. Except for the boundary surfaces and regions close to the insulated bottom where the solid phase and fluid temperatures are the same, the solid phase temperature is always higher than the fluid temperature. Therefore, heat is always transferred from the solid particles to the fluid, so the solid particles act as fins and at the same time intensify the fluid mixing which also enhances the convection heat transfer.

It is quite interesting to compare the temperature distributions in the sintered porous media shown here and in the non-sintered porous media shown in Jiang [8]. For non-sintered metallic porous structures where $\lambda_s \gg \lambda_f$, the predictions made using the local thermal non-equilibrium model [8] showed that the solid phase temperature near the upper wall was much lower than the fluid temperature, while in most other parts of the porous channel the solid phase temperature was higher than the fluid temperature. Therefore, in non-sintered porous media, the thermal contact resistance between the particles and the wall caused the solid particle temperature near the upper boundary to be lower than the surrounding fluid temperature, i.e., part of the heat was transferred first to the fluid and then from the fluid to the solid particles near the upper wall. In the middle of the porous media channel, heat was transferred from the solid phase to the fluid. Obviously, the role of the heat conduction or the fin effect of the solid particles in non-sintered porous plate channels is not as effective as in sintered porous media. This is an important reason for the lower heat transfer coefficients in non-sintered porous channel than in sintered porous media.

As mentioned earlier, the porosity at the wall and the thermal contact resistance between particles and between the particles and the wall are important factors

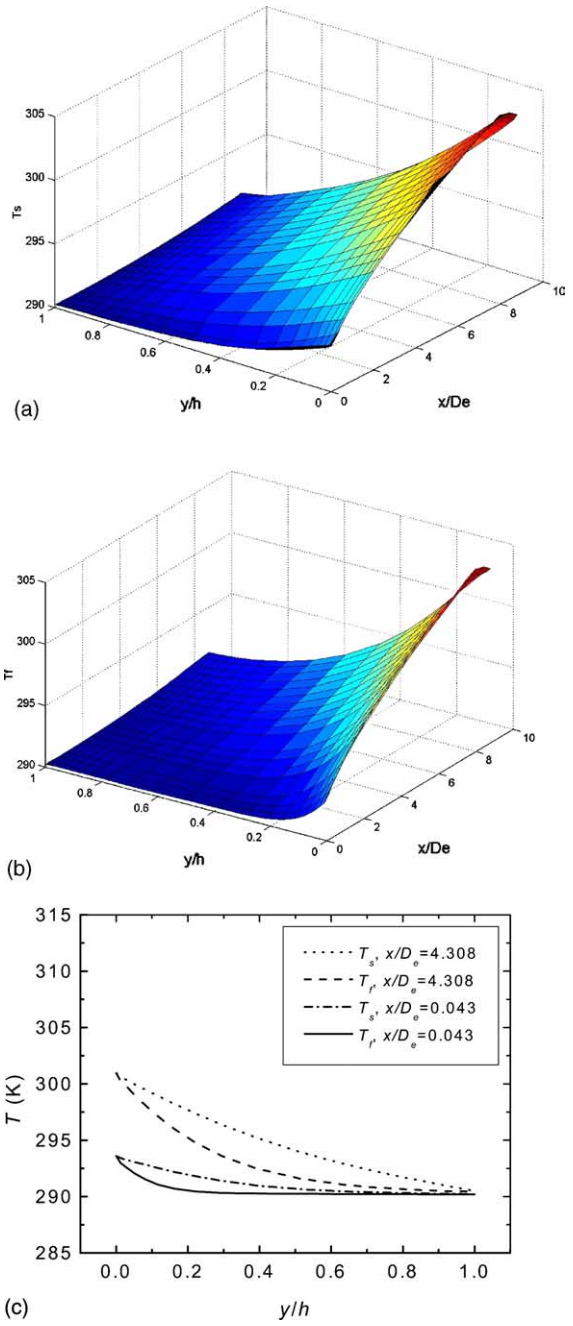

Fig. 9. Numerical simulation of the temperature field for convection heat transfer of water in sintered porous media: (a) solid phase temperature field; (b) fluid temperature field; (c) solid phase and fluid temperature distributions ($d_p = 0.5$–0.71 mm, $Re_D = 167$, $q_w = 1.981 \times 10^4$ W/m^2, $t_{f0} = 17.5$ °C).

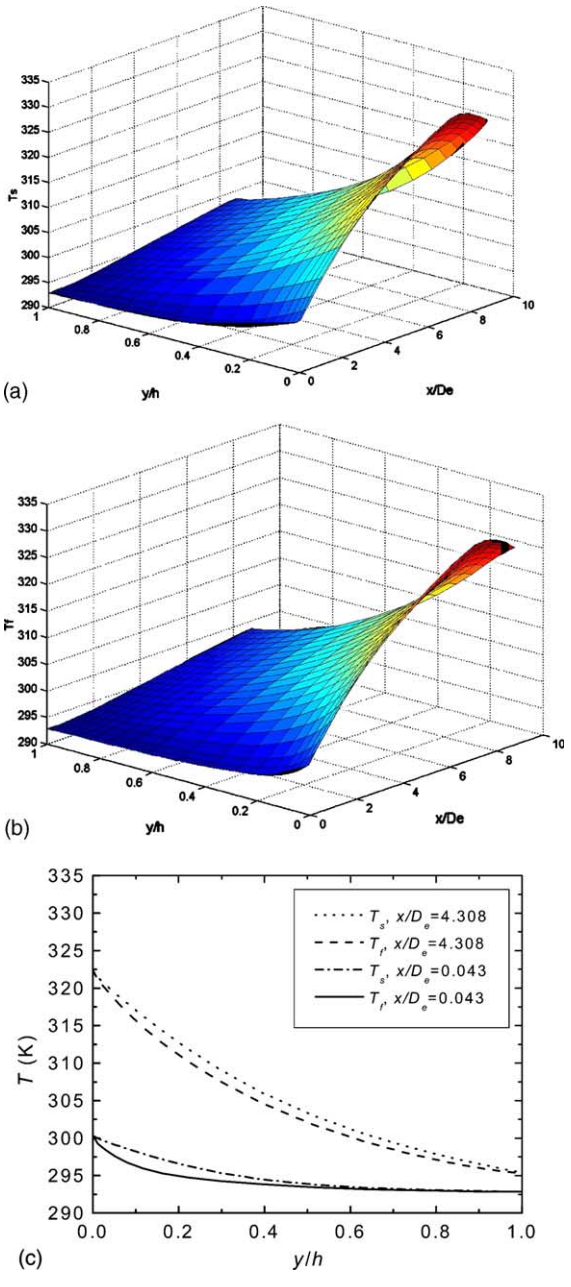

Fig. 10. Numerical simulation of the temperature field for convection heat transfer of air in sintered porous media: (a) solid phase temperature field; (b) fluid temperature field; (c) solid phase and fluid temperature distributions ($d_p = 0.5$–0.71 mm, $Re_D = 2840$, $q_w = 6.808 \times 10^3$ W/m^2, $t_{f0} = 20.8$ °C).

affecting the convection heat transfer in the porous plate channel. For sintered metallic porous media, the porosity at the wall and the thermal contact resistance are less than that in non-sintered porous media; therefore, the heat transport from the wall to the middle of the porous layer is greater which will enhance the overall heat transfer coefficient on the plate wall. The heat transfer with air is obviously less than with water; therefore, the influence of the porosity at the wall and the thermal contact resistance on the overall convection

heat transfer is more evident for air. Experimental research [24] has also showed that the convection heat transfer of air in sintered porous media is much more intensive than in non-sintered porous media.

5. Conclusions

(1) For convection heat transfer in sintered porous media, the thermal boundary conditions on the heated wall surface should be that the particle temperatures are equal to the fluid temperatures due to the reduced thermal resistance and the increased mixing resulting from the sintering process.
(2) The wall porosity in sintered porous media is less than that in non-sintered porous media, which increases the convection heat transfer in sintered porous media.
(3) The wall effect reduces the heat transfer coefficient near the front of the heated section and slightly increases the heat transfer coefficient near the heated section outlet.
(4) Numerical simulations of convection heat transfer of air and water in sintered bronze porous media using the local thermal non-equilibrium model and the variable porosity model with consideration of the wall effect at the inlet and outlet corresponded well with the experimental data.

Acknowledgements

The project was supported by the National Outstanding Youth Fund from the National Natural Science Foundation of China (No. 50025617) and the Major State Basic Research Development Program (No. G1999033106). We also thank Dr. David Christopher for editing the English.

References

[1] K. Vafai, C.L. Tien, Boundary and inertial effects on flow and heat transfer in porous media, Int. J. Heat Mass Transfer 24 (1981) 195–203.
[2] J.L. Lage, The fundamental theory of flow through permeable media from Darcy to Turbulence, in: D.B. Ingham, I. Pop (Eds.), Transport Phenomena in Porous Media, Pergamon, Oxford, 1998, pp. 1–30.
[3] C.T. Hsu, P. Cheng, Thermal dispersion in a porous medium, Int. J. Heat Mass Transfer 33 (1990) 1587–1597.
[4] M. Sozen, K. Vafai, Longitudinal heat dispersion in porous beds with real gas flow, J. Thermophys. Heat Transfer 7 (1) (1993) 153–157.
[5] S.M. Kuo, C.L. Tien, Transverse dispersion in packed sphere bed, in: ASME Proc. 25th National Heat Transfer Conf., Houston, TX, 1988, pp. 629–634.
[6] N. Wakao, S. Kaguei, Heat and Mass Transfer in Packed Beds, Gordon and Breach, New York, 1982.
[7] T. Masuoka, Y. Takatsu, Turbulence model for flow through porous media, Int. J. Heat Mass Transfer 39 (13) (1996) 2803–2809.
[8] P.X. Jiang, Z.P. Ren, B.X. Wang, Numerical simulation of forced convection heat transfer in porous plate channels using thermal equilibrium and non-thermal equilibrium models, Numer. Heat Transfer, Part A 35 (1999) 99–113.
[9] P.X. Jiang, M. Li, Z.P. Ren, Forced convection heat transfer in plate channels filled with packed beds or sintered porous media, Tsinghua Sci. Technol. 7 (2) (2002) 202–208.
[10] J.L. Lage, The implications of the thermal equilibrium assumption for surrounding-driven steady conduction within a saturated porous medium layer, Int. J. Heat Mass Transfer 42 (1999) 477–485.
[11] A. Amiri, K. Vafai, Analysis of dispersion effects and non-thermal equilibrium, non-Darcian, variable porosity incompressible flow through porous media, Int. J. Heat Mass Transfer 37 (6) (1994) 939–954.
[12] A. Amiri, K. Vafai, T.M. Kuzay, Effects of boundary conditions on non-Darcian heat transfer through porous media and experimental comparisons, Numer. Heat Transfer, Part A 27 (1995) 651–664.
[13] M. Quintard, Modeling local non-equilibrium heat transfer in porous media, Heat Transfer 1998, in: Proc. 11th Int. Heat Transfer Conf., Kyongju, Korea, vol. 1, 1998, pp. 279–285.
[14] G.P. Peterson, C.S. Chang, Two-phase heat dissipation utilizing porous-channels of high-conductivity materials, J. Heat Transfer 120 (1998) 243–252.
[15] A.R. Martin, C. Saltiel, W. Shyy, Heat transfer enhancement with porous inserts in recirculating flows, J. Heat Transfer 120 (1998) 458–467.
[16] D.Y. Lee, K. Vafai, Analytical characterization and conceptual assessment of solid and fluid temperature differences in porous media, Int. J. Heat Mass Transfer 42 (1999) 423–435.
[17] W.H. Hsieh, S.F. Lu, Heat-transfer analysis and thermal dispersion in thermally-developing region of a sintered porous metal channel, Int. J. Heat Mass Transfer 43 (2000) 3001–3011.
[18] P.X. Jiang, Z.P. Ren, Numerical investigation of forced convection heat transfer in porous media using a thermal non-equilibrium model, Int. J. Heat Fluid Flow 22 (1) (2001) 102–110.
[19] P.X. Jiang, G.S. Si, M. Li, Z.P. Ren, Forced convection heat transfer of air in a porous plate channel, in: Proc. 5th Beijing Int. Conf. Heat Transfer, Aug. 6–10, Beijing, 2000, pp. 492–497.
[20] B. Alazmi, K. Vafai, Constant wall heat flux boundary conditions in porous media under local thermal non-equilibrium conditions, Int. J. Heat Mass Transfer 45 (2002) 3071–3087.
[21] P.X. Jiang, Analysis of the thermal characteristics on the boundary in porous media, in: Proc. National Heat and Mass Transfer Conf., Qingdao, Shandong, 2001, pp. 514–518 (in Chinese).
[22] P.X. Jiang, Z. Wang, Z.P. Ren, B.X. Wang, Experimental research of forced convection heat transfer in plate channel filled with glass or metallic particles, Exp. Therm. Fluid Sci. 20 (1999) 45–54.

[23] G.J. Hwang, C.H. Chao, Heat transfer measurement and analysis for sintered porous channels, J. Heat Transfer 116 (1994) 456–464.
[24] P.X. Jiang, M. Li, T.J. Lu, L. Yu, Z.P. Ren, Experimental research on convection heat transfer in sintered porous plate channels, Int. J. Heat Mass Transfer, in press.
[25] M.L. Hunt, C.L. Tien, Non-Darcy convection in cylindrical packed beds, J. Heat Transfer 110 (1988) 378–384.
[26] P. Cheng, C.T. Hsu, Fully-developed forced convective flow through an annular packed-sphere bed with wall effects, Int. J. Heat Mass Transfer 29 (1986) 1843–1853.
[27] E. Achenbach, Heat and flow characteristics of packed beds, Exp. Therm. Fluid Sci. 10 (1995) 17–27.
[28] K.K. Kar, A. Dybbs, Internal heat transfer coefficients of porous metals, in: ASME Proc. Winter Annual Meeting, Phoenix, AZ, 1982, pp. 81–91.